IJSGS VOL. 8 (1), MARCH 2022 https://doi.org/10.57233/ijsgs.v8i1.317 URL: https://fugus-ijsgs.com.ng

IJSGS

ISSN: 2488-9229
FEDERAL UNIVERSITY
GUSAU-NIGERIA

INTERNATIONAL JOURNAL OF SCIENCE FOR GLOBAL SUSTAINABILITY

Unsteady Convective Couette Flow with Heat Source

Omokhuale E.[1] and Jabaka M. L.[2]

[1]Department of Mathematical Sciences, Federal University Gusau, P. M. B. 1001, Zamfara State, Nigeria.
[2]Department of Computer Science, Federal University Gusau, P. M. B. 1001, Zamfara State, Nigeria.

Corresponding Authors' Email: emmanuelomokhuale@yahoo.com

Received on: January, 2022 **Revised and Accepted on:** February, 2022 **Published on:** March 2022

ABSTRACT

The effect of heat source on unsteady hydromagnetic convective Couette flow of a viscous, electrically conducting and incompressible fluid is investigated. The governing equations that explain the flow formation are modeled as Partial Differential Equations (PDEs) and solved numerically by Finite Element Method (FEM). The influence of physical parameters on the fluid velocity, temperature and concentration were presented graphically and discussed. It is seen that, the momentum and temperature boundary layers are significantly influenced as the value of heat source parameter is increased while an opposite trend is observed on the velocity as Hatman number is increased.

Keywords: Couette flow; Convective: porous medium; FEM; MHD and Heat source.

Nomenclatures and Greek Symbols

Symbol	Interpretation	Unit
y'	Dimensional length	m
Y	Dimensionless length	
g	Gravitational acceleration	ms^{-2}
k_0	Thermal conductivity	W/mK
T'	Dimensional temperature	K
d	Dimensional channel width	m
T_d'	Ambient temperature	K
u', v'	Dimensional velocity	ms^{-1}
υ	Kinematic viscosity	m^2s^{-1}
C_p	Specific heat at constant pressure	kJ/kgK
Q_0	Volumetric rate of heat generation/absorption	J
S	Constant heat source parameter	
Pr	Prandtl number	
Sc	Schmidt number	
t'	Dimensional time	s
t	Dimensionless time	
U	Dimensionless velocity	
T	Dimensionless temperature of the fluid	
C	Dimensionless temperature of the fluid	
M	Hatman number	
Rc	Chemical reaction parameter	
Dr	Dufour Number	
β	Coefficient of thermal expansion	$1/K$
β'	Coefficient of thermal expansion	$1/K$
μ	Coefficient of viscosity	Ns/m^2
μ_e	Kinematic viscosity of the fluid	m^2/s

ρ	Fluid density	kg/m^3
σ	Stefan-Boltzman Constant	JK^{-1}

1.0 INTRODUCTION

Heat source/sink is a significant factor for fluid flow because it has essential usefulness in the field of food industry, physics thermal and mechanical engineering processes named as heat treatment, ventilation and air conditioning. Food processing operations also involve cooling and heating processes (Anwar *et al.*, 2020).

Couette flow in fluid dynamics refers to the laminar flow of viscous fluid in the space between two parallel plates, one of which moving relative to the other. The flow is driven by virtue of viscous drag force acting on the fluid and the applied pressure gradient parallel to the plates. This type of flow is named in honor of Maurice Marie Alfred Couette, a Professor of Physics at the French University of Angers in the late 19th century. Couette flow is frequently used in undergraduate physics and engineering courses to illustrate shear – driven fluid motion. Some important applications of Couette motion are magnetohydrodynamic power generators and pumps, polymer technology, petroleum industry and purification of crude oil and fluid droplets sprays.

Das and Bera (2014) obtained analytically solutions of hydromagnetic convective Couette flow in presence of time dependent suction and radiative heat source by perturbation method. The numerical solution of natural convection in unsteady hydromagnetic Couette flow of viscous incompressible electrically conducting fluid between two vertical parallel plates in the presence of thermal radiation was obtained by Rao *et al.* (2014). Kesavaiah *et al.* (2013) studied free convection in unsteady Couette flow of a viscous incompressible fluid in the presence of thermal radiation and heat source. Unsteady MHD convective Couette flow of a viscous, incompressible, electrically conducting and time dependent heat absorbing fluid was examined by Seth *et al.* (2016). They obtained an exact solution for the fluid velocity and temperature in closed form by Laplace transform technique. Unsteady three-dimensional Couette flow of a viscous incompressible fluid between two porous plates analytically was studied by Loganathan and Gomathi (2016). Sharma *et al.* (2021) researched on entropy generation and their minimization for magnetohydrodynamic oscillatory Couette flow through a vertical channel in the existence of heat source and thermal radiation.

On the other hand, FEM is a numerical technique used to obtain an approximate solution to boundary value problems as they consist of elliptic partial differential equations and the boundary conditions. It has been applied to many physical problems. The method basically consists of assuming the piecewise continuous function for the solution and obtaining the parameters of the functions in a manner that reduces the error of the solution. Using FEM, Job and Gunakala (2015) studied unsteady radiative MHD natural convection Couette flow between permeable plates. Raju *et al.* (2016) studied unsteady hydromagnetic natural convection Couette flow of a viscous, incompressible and electrically conducting fluid between two vertical plates in the presence of thermal radiation using finite element method. The entropy generation and temperature dependent heat source effects on MHD Couette flow with permeable base in the presence of radiation and viscous dissipation was studied by Sukumar and Varma (2016). Reddy *et al.* (2017) investigated unsteady MHD heat transfer in Couette flow of water at 4^{O}C in a rotating system with ramped temperature. Ajibade and Bichi (2019) examined natural convection Couette flow through a vertical porous channel due to combined effects of thermal radiation and variable fluid properties. Recently, Xia (2021) reported gear-generalized differential quadrature analysis of oscillatory convective Taylor-Couette flows. Bilal *et al.* (2021) worked on Couette flow of viscoelastic dusty fluid in a rotating frame with the heat transfer. Sharma *et al.* (2022) investigated dissipative MHD oscillatory unsteady free convective flow in a vertical channel in the presence of heat source effect and thermal radiation.

Motivated by the above studies and applications, a novel investigation has been conducted to study unsteady convective Couette flow in the presence

of thermal radiation and heat sink. The flow is governed by a modeled coupled nonlinear system of partial differential equations (PDEs) in dimensional form which are transformed into non-dimensional form using some suitable non-dimensional variables. The resulting equations whose exact solutions if possibly found is difficult to get Thus, we numerically used FEM to obtain the solutions. Furthermore, the effects of physical parameters embedded in the problem were examined with the help of graphs.

2.0 PHYSICAL FORMULATION

The two- dimensional unsteady convective Couette flow of an electrically conducting and viscous fluid between two parallel plates $y=0$ and $y=a$ surrounded by porous medium under the influence of a uniform transverse magnetic field, thermal radiation and heat source. The following assumptions are considered:

(i) The x'- axis and y'- axis are considered in the vertically upward and normal direction to the plate respectively.

(ii) The plates be separated by a distance d. Initially, at time $t' \le 0$, the fluid and the plates of the channel are assumed to be at rest and at same temperature T_a' and concentration C_a'. When time $t' > 0$, the plate (at $y' = 0$) begins to move with time dependent velocity $U_0 t'^n$ (U_0 is a constant and is a non-negative integer) in its own plane and at the same time the plate temperature and concentration is raised to T_w' and C_w' respectively while the plate (at $y' = a$) is fixed. Similarly, at $t' > 0$, the wall at $y' = a$ is stationary and kept at a constant *temperature* and concentration T_a' and C_a' respectively.

(iii) The transverse magnetic field of the uniform strength H_0 is to be applied to the plate,

(iv) The fluid has constant suction, kinematic viscosity and thermal conductivity, the Boussinesq approximations has been considered for the flow.

From the above assumptions, the flow is governed by the following PDEs;

Continuity equation:

$$\frac{\partial v'}{\partial y'} \tag{1}$$

Momentum equation:

$$v\frac{\partial^2 u'}{\partial y'^2} - \frac{\partial u'}{\partial t'} + g\beta_1\left(T' - T_a'\right) + g\beta_2\left(T' - T_a'\right) - \frac{\nu u'}{K'} - \frac{\sigma\mu_e^2 B_0^2}{\rho}\left(u' - U_0 t'^n\right) = 0 \tag{2}$$

Energy equation:

$$\frac{k_0}{\rho Cp}\frac{\partial^2 T'}{\partial y'^2} - \frac{\partial T'}{\partial t'} + Q_0\left(T' - T_a\right) = 0 \tag{3}$$

Species diffusion equation:

$$Dc\frac{\partial^2 C'}{\partial y'^2} - \frac{\partial C'}{\partial t'} - Rc\left(C' - C_a'\right) = 0 \tag{4}$$

The corresponding initial and boundary conditions are:

$$\left.\begin{aligned} t' \le 0 &: u' = 0, T' = T_a', C' = C_a' \quad for \;\; 0 \le y' \le a \\ t' > 0 &: \begin{cases} u' = U_0 t'^n, T' = T_a', C' = C_a' & at\; y' = 0 \\ u' = 0, T' = T_a', C' = C_a' & at\;\; y' = a \end{cases} \end{aligned}\right\} \tag{5}$$

To get the non-dimensional form of Equations (1), (3) and (8), the following dimensionless quantities are introduced:

$$\left.\begin{aligned} U=\frac{u^*}{a},Y=\frac{y^*}{a},t=\frac{t^*\nu}{a^2},T=\frac{T^*-T_a^*}{T_w^*-T_a^*},C=\frac{C^*-C_a^*}{C_w^*-C_a^*},\\ Gr=\frac{g\beta_T\left(T_w^*-T_a^*\right)}{\nu},Gc=\frac{g\beta_m\left(C_w^*-C_a^*\right)}{\nu},F=\frac{U_0a^{2n-1}}{\nu^n}\\ M^2=\frac{\sigma\mu_e^2B_0^2a^2}{\rho\nu},\Pr=\frac{\rho\nu Cp}{k_0},Sc=\frac{\nu}{D},\mathrm{Re}_x^{-1}=\frac{U_0x^*}{\nu} \end{aligned}\right\} \quad (6)$$

Using the dimensionless quantities in Equation (6), the dimensionless form of Equations (1), (3) and (8) and (3) are:

$$\frac{\partial^2U}{\partial Y^2}-\frac{\partial U}{\partial t}+GrT+GcC-M^2\left(U-Ft^n\right)=0 \quad (7)$$

$$\frac{1}{\Pr}\frac{\partial^2T}{\partial Y^2}-\frac{\partial T}{\partial t}+ST=0 \quad (8)$$

$$\frac{1}{Sc}\frac{\partial^2C}{\partial Y^2}-\frac{\partial C}{\partial t}-RcC=0 \quad (9)$$

initial and boundary conditions (4) in dimensionless forms are:

$$\left.\begin{aligned} t\le 0: U=0,T=0,C=0 \quad for \quad 0\le Y\le a\\ t>0:\begin{cases} U=Ft^n,T=1,C=1 \quad at\, Y=0\\ U=0,T=0,C=0 \quad at\ Y=a \end{cases} \end{aligned}\right\} \quad (10)$$

Two cases are studied, to find the solutions of Equations (7) to (9) subject to the initial and boundary conditions (10):

1. Impulsive movement of the plate at $Y=0$ (i.e., $n=0$) and
2. Uniform accelerated movement of the plate at $Y=0$ (i.e., $n=1$).

Case (1): Impulsive movement of the plate at $Y=0$:

Taking $n=0$ in Equation (7), then the Equation (7) can be expressed as

$$\frac{\partial^2U}{\partial Y^2}-\frac{\partial U}{\partial Y}+GrT+GcC-M^2\left(U-F\right)=0 \quad (11)$$

and the corresponding boundary conditions (10) reduce to

$$\left.\begin{aligned} t\le 0: U=0,T=0,C=0 \quad for \quad 0\le Y\le d\\ t>0:\begin{cases} U=F,T=1,C=1 \quad at\, Y=0\\ U=0,T=0,C=0 \quad at\ Y=a \end{cases} \end{aligned}\right\} \quad (12)$$

Case (2): Uniform accelerated movement of the plate at $Y=0$.

Taking $n=1$ in Equation (7), then the Equation (7) can be written as

$$\frac{\partial^2U}{\partial Y^2}-\frac{\partial U}{\partial Y}+GrT+GcC-M^2\left(U-Ft\right)=0 \quad (13)$$

and the initial and boundary conditions (10) reduce to

$$\left.\begin{aligned} t \le 0 : U = 0, T = 0, C = 0 \quad for \quad 0 \le Y \le a \\ t > 0 : \begin{cases} U = Ft, T = 1, C = 1 \quad at\, Y = 0 \\ U = 0, T = 0, C = 0 \quad at\ Y = a \end{cases} \end{aligned}\right\} \tag{14}$$

For practical engineering applications and the design of chemical engineering systems, quantities of interest viz. Skin-friction, Nusselt and Sherwood numbers which are necessary to compute. The skin-friction or the shear tress at the moving plate of the channel in dimensionless form is given by

$$\tau = -\left(\frac{\tau_w^*}{\rho u_0 \nu}\right)_{y'=0} = -\left(\frac{\partial U}{\partial Y}\right)_{y'=0} \tag{15}$$

The rate of heat transfer at the moving hot plate of the channel in dimensionless form is illustrated by

$$Nu_0 = -x' \frac{\left(\frac{\partial T'}{\partial Y'}\right)_{y'=0}}{T_w' - T_a'} \Rightarrow Nu_0 \,\mathrm{Re}_x^{-1} = -\left(\frac{\partial T}{\partial Y}\right)_{Y=0} \tag{16}$$

Also, the rate of heat transfer on the stationary plate is given by

$$Nu_1 = -x' \frac{\left(\frac{\partial T'}{\partial Y'}\right)_{y'=a}}{T_w' - T_a'} \Rightarrow Nu_1 \,\mathrm{Re}_x^{-1} = -\left(\frac{\partial T}{\partial Y}\right)_{Y=1} \tag{17}$$

The Sherwood number at the moving plate of the channel in dimensionless form is given by

$$Sh = -x' \frac{\left(\frac{\partial C'}{\partial Y'}\right)_{y'=0}}{C_w' - C_a'} \Rightarrow Sh\,\mathrm{Re}_x^{-1} = -\left(\frac{\partial C}{\partial Y}\right)_{Y=0} \tag{18}$$

where Re_x is the Reynold's number. The mathematical modeling of the problem is now done. So, Equations. (11), (12), (14) and (16) presents a coupled system of linear PDEs and these are to be solved with initial and boundary conditions (15) and (17). Therefore, finding the exact solutions are complicated, whenever it is possible. Thus, these equations are solved numerically by FEM.

3.0 NUMERICAL SOLUTIONS BY FEM

The FEM is an efficient numerical and computational method to solving a variety of engineering and real-world problems. So many developers, researchers and users have recognized this method as one of the most powerful numerical analysis tools useful to analyze complex engineering problems. The simplicity, flexibility, computability and accuracy of the method make it significant in modeling and design process. This is because of the discretization of domain of the problem is done employing highly flexible elements or uniform or non-uniform patches that can be easily shown as complex shapes. The method vitally comprises the piecewise continuous functions in a systematic way that reduces the error in the solution.

The steps involved in the finite element analysis as follows:

Step 1: Discretization of the domain
Step 2: Generation of the element equations
Step 3: Assembling of the element equations
Step 4: Imposition of the boundary conditions
Step 5: Solution of assembled equations

Variational Formulation

The Variational formulation associated with Equations (10) to (12) over a typical two-noded linear element $\left(Y_e, Y_{e+1}\right)$ is given by

$$\int_{Y_e}^{Y_{e+1}} z_1\left[\left(\frac{\partial U}{\partial t}\right)-\left(\frac{\partial^2 U}{\partial y^2}\right)-Gr(T)-Gc(C)+M^2\left(U-Ft^n\right)\right]dy=0 \tag{19}$$

$$\int_{Y_e}^{Y_{e+1}} z_2\left[\left(\frac{\partial T}{\partial t}\right)-\frac{1}{\Pr}\left(\frac{\partial^2 T}{\partial y^2}\right)\right]dy=0 \tag{20}$$

$$\int_{Y_e}^{Y_{e+1}} z_3\left[\left(\frac{\partial C}{\partial t}\right)-\frac{1}{Sc}\left(\frac{\partial^2 C}{\partial y^2}\right)\right]dy=0 \tag{21}$$

where z_1, z_2 and z_3 are arbitrary test functions and may be seen as the variation in U, T and C respectively. When the order of integration was reduced, we got the following system of equation:

$$\int_{Y_e}^{Y_{e+1}} z_1\left[z_1\left(\frac{\partial U}{\partial t}\right)+\left(\frac{\partial z_1}{\partial y^2}\right)\left(\frac{\partial U}{\partial y}\right)+(M^2)(z_1)U-(F)(z_1)t^n-(Gr)(z_1)T-(Gc)(z_1)C\right]dy$$
$$-\left[(z_1)\left(\frac{\partial u}{\partial y}\right)\right]_{Y_e}^{Y_{e+1}}=0 \tag{22}$$

$$\int_{Y_e}^{Y_{e+1}}\left[(z_2)\left(\frac{\partial T}{\partial t}\right)+\frac{1}{\Pr}\left(\frac{\partial z_2}{\partial y}\right)\left(\frac{\partial T}{\partial y}\right)\right]dy-\left[\left(\frac{z_2}{\Pr}\right)\left(\frac{\partial T}{\partial y}\right)\right]_{Y_e}^{Y_{e+1}}=0 \tag{23}$$

$$\int_{Y_e}^{Y_{e+1}}\left[(z_3)\left(\frac{\partial C}{\partial t}\right)+\frac{1}{Sc}\left(\frac{\partial z_3}{\partial y}\right)\left(\frac{\partial C}{\partial y}\right)\right]dy-\left[\left(\frac{z_3}{Sc}\right)\left(\frac{\partial C}{\partial y}\right)\right]_{Y_e}^{Y_{e+1}}=0 \tag{24}$$

Finite Element Formulation:

The finite element model can be gotten from Equations (25) to (27) by substituting the finite element approximations of the form:

$$U=\sum_{k=1}^{2}U_k^e\xi_k^e, T=\sum_{k=1}^{2}T_k^e\xi_k^e \text{ and } \sum_{k=1}^{2}C_k^e\xi_k^e \tag{25}$$

with $z_1=z_2=z_3=\xi_k^e(k=1,2)$, U_k^e, T_k^e and C_k^e are the velocity, temperature and concentration respectively at the k^{th} node of typical e^{th} element (Y_e, Y_{e+1}) and ξ_k^e are the shape functions for this element (Y_e, Y_{e+1}) and are taken as:

$$\xi_1^e=\frac{Y_{e+1}-Y}{Y_{e+1}-Y_e} \text{ and } \xi_2^e=\frac{Y-Y_e}{Y_{e+1}-Y_e},\ Y_e\le Y\le Y_{e+1} \tag{26}$$

This finite element model of the equations for

$$\begin{bmatrix}[P^{11}] & [P^{12}] & [P^{13}]\\ [P^{21}] & [P^{22}] & [P^{23}]\\ [P^{31}] & [P^{32}] & [P^{33}]\end{bmatrix}\begin{bmatrix}\{U^e\}\\ \{T^e\}\\ \{C^e\}\end{bmatrix}+\begin{bmatrix}[W^{11}] & [W^{12}] & [W^{13}]\\ [W^{21}] & [W^{22}] & [W^{23}]\\ [W^{31}] & [W^{32}] & [W^{33}]\end{bmatrix}\begin{bmatrix}\{U'^e\}\\ \{T'^e\}\\ \{C'^e\}\end{bmatrix}=\begin{bmatrix}\{a^{1e}\}\\ \{a^{2e}\}\\ \{a^{3e}\}\end{bmatrix} \tag{27}$$

where $\{\{P^{mn}\},\{W^{mn}\}\}$ and $\{\{U^e\},\{T^e\},\{C^e\},\{U'^e\},\{T^e\},\{C^e\},\{a^{me}\}\}(m=1,2,3)$ are the set of matrices of order 2×2 and 2×1 respectively and $'$ (dash) indicates $\frac{d}{dy}$.

These matrices are defined as follows:

$$P^{11}_{Ik} = \int_{Y_e}^{Ye+1}\left[\left(\frac{\partial \xi_i^e}{\partial y}\right)\left(\frac{\partial \xi_k^e}{\partial y}\right)\right]dy + \left(M^2\right)\int_{Y_e}^{Ye+1}\left[\left(\xi_i^e\right)\left(\xi_k^e\right)\right]dy - Ft^n\int_{Y_e}^{Ye+1}\left(\xi_i^e\right)dy,$$

$$P^{12}_{ik} = -Gr\int_{Y_e}^{Ye+1}\left[\left(\xi_i^e\right)\left(\xi_k^e\right)\right]dy, P^{13}_{ik} = -Gc\int_{Y_e}^{Ye+1}\left[\left(\xi_i^e\right)\left(\xi_k^e\right)\right]dy, W^{11}_{ik} = \int_{Y_e}^{Ye+1}\left[\left(\xi_i^e\right)\left(\xi_k^e\right)\right]dy, W^{12}_{ik} = W^{13}_{ik} = 0,$$

$$W^{21}_{ik}, W^{23}_{ik} = 0, W^{31}_{ik} = W^{32}_{ik} = 0, P^{21}_{ik} = 0, P^{31}_{ik} = 0, b^{1e}_i = \left[\left(\xi_i^e\right)\left(\frac{\partial U}{\partial Y}\right)\right]_{Y_e}^{Y_{e+1}}$$

$$P^{22}_{ik} = \frac{1}{\Pr}\int_{Y_e}^{Ye+1}\left[\left(\frac{\partial \xi_i^e}{\partial Y}\right)\left(\frac{\partial \xi_k^e}{\partial Y}\right)\right]dy, P^{23}_{ik},$$

$$P^{33}_{ik} = \frac{1}{Sc}\int_{Y_e}^{Ye+1}\left[\left(\frac{\partial \xi_i^e}{\partial Y}\right)\left(\frac{\partial \xi_k^e}{\partial Y}\right)\right]dy, W^{22}_{ik}\int_{Y_e}^{Ye+1}\left[\left(\xi_i^e\right)\left(\xi_k^e\right)\right]dy, a^{2e}_i = \left[\left(\frac{\xi_i^e}{\Pr}\right)\left(\frac{\partial T}{\partial Y}\right)\right]_{Y_e}^{Y_{e+1}},$$

$$P^{32}_{ik} = Sr\int_{Y_e}^{Ye+1}\left[\left(\frac{\partial \xi_i^e}{\partial Y}\right)\left(\frac{\partial \xi_k^e}{\partial Y}\right)\right]dy,$$

$$a^{3e}_i = \left[\left(\frac{\xi_i^e}{Sc}\right)\left(\frac{\partial C}{\partial Y}\right)\right]_{Y_e}^{Y_{e+1}} \text{ and } W^{33}_{ik} = \int_{Y_e}^{Ye+1}\left[\left(\xi_i^e\right)\left(\xi_k^e\right)\right]dy.$$

In one-dimensional space, linear element, quadratic element or element of higher order can be used. The entire flow domain is divided into 10,000 quadratic elements of equal size. Each element is three-noded, and as such the whole domain contains 20,001 nodes. At each node, three functions are to be evaluated: hence, after assembling of the element equations, we got a system of 80,004 equations which are linear. Thus, an iterative scheme must be employed in the solution. On imposing the boundary conditions, a system of equations was gotten which is solved by Gauss elimination method while maintaining an accuracy of 0.00001. A convergence criterion based on the relative difference between the current and previous iterations is used. After these differences satisfy the desired accuracy, the solution is assumed to have been converged and iterative process terminated. The Gaussian quadrature is implemented for solving the integrations. The code of the algorithm has been executed twice in MAPLE for cases 1 and 2. Excellent results was seen for all results.

Study of grid Independence

In general, to study the grid independency/dependency, the mesh size is varied in order to check the solution at different mesh (grid) sizes and get a range at which there is no variation in the solutions.

4.0 RESULTS AND DISCUSSION

A MAPLE program is written to generate line graphs for the velocity, temperature and concentration profiles in other to provide a clear understanding of the problem at hand. Figures 1 and 2 show the effects of thermal and mass Grashof numbers on the velocity profiles. It is found that, there is increase in the velocity due to the enhancement of thermal buoyancy force. Also, the peak value of the velocity increases rapidly near the porous plate and the decays smoothly for free steam velocity. It is further noted that the fluid velocity increases and the peak value is more distinctive due to increase in species buoyancy force. Thus, the velocity distribution attains a distinctive maximum value in the vicinity of the plate and then reduces properly to approach free stream value. The effect of Hartmann number on the velocity profiles is as shown in Figure 3. It is seen that, the velocity of the fluid falls with increasing magnetic parameter. This

type of resistive force has a tendency to slow down the flow field. This is because the presence of magnetic field in an electrically conducting fluid sets in a force called Lorentz force which acts against the flow if the magnetic field is applied in the normal direction as reflected in the problem.

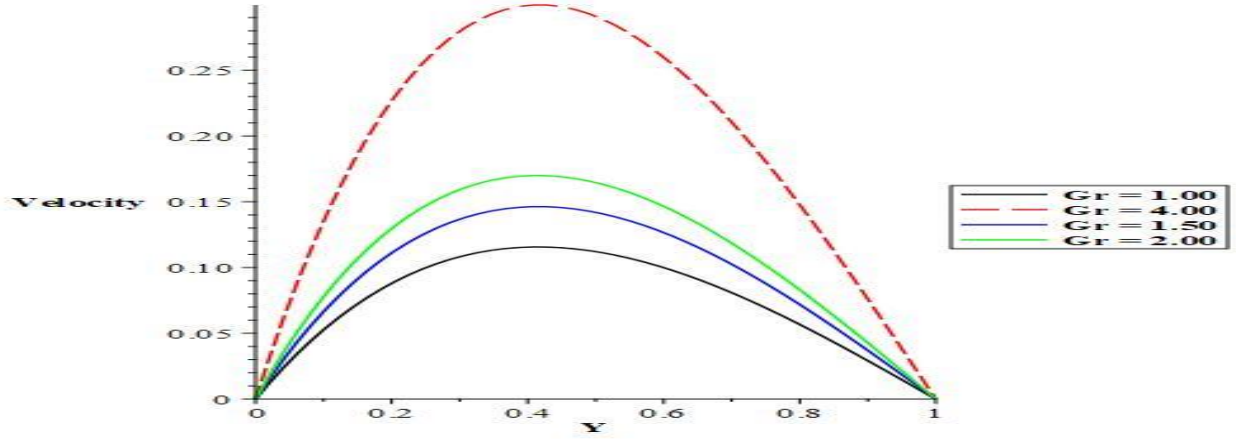

Figure 1: Effect of Gr on velocity profiles.

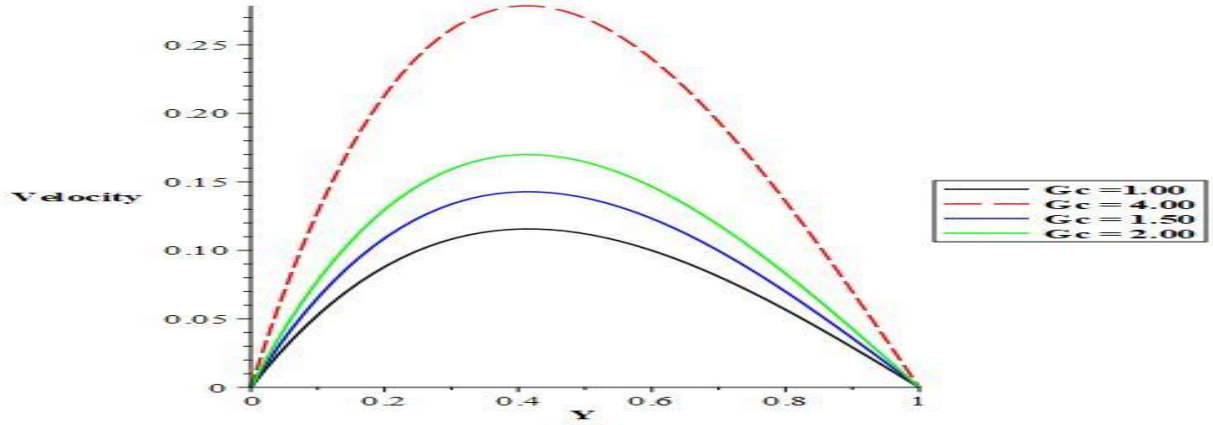

Figure 2: Effect of Gc on velocity profiles.

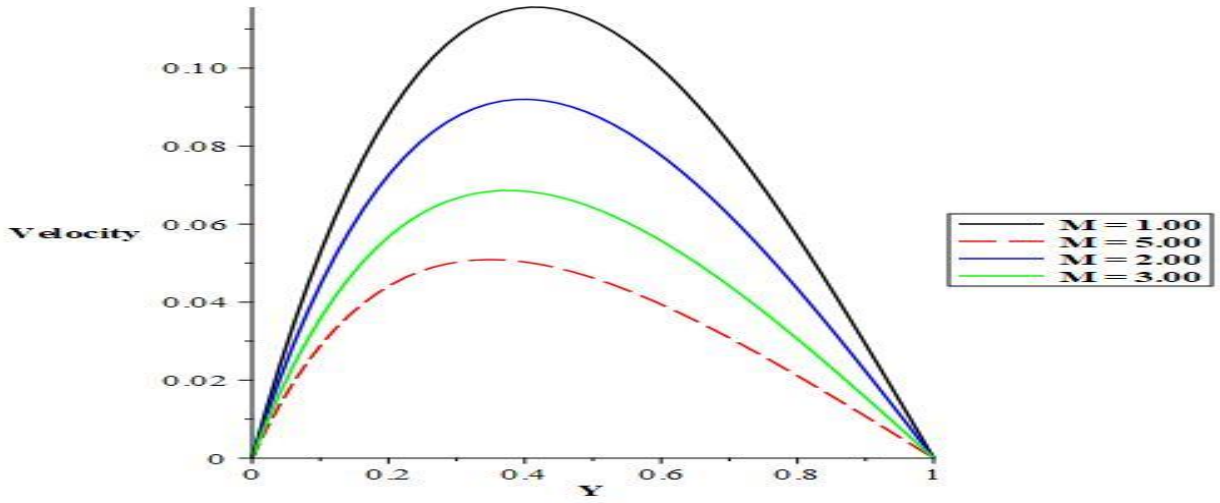

Figure 3: Effect of M on velocity profiles.

It is noticed from Figure 4 that, significance in heat source causes rise in the fluid velocity profile. Figure 5 provides the effect of Prandtl number on the velocity profiles. From this Figure, it is obvious that the velocity reduces as the values of Prandtl number is rises. Physically, this happens due to the phenomenon that fluid with high Prandtl number have greater viscosity, which makes the fluid thick and then move slowly. Figures 6 illustrates the velocity profiles for different values of Schmidt number. It is observed that, an increase in Schmidt number lowers the velocity boundary layer.

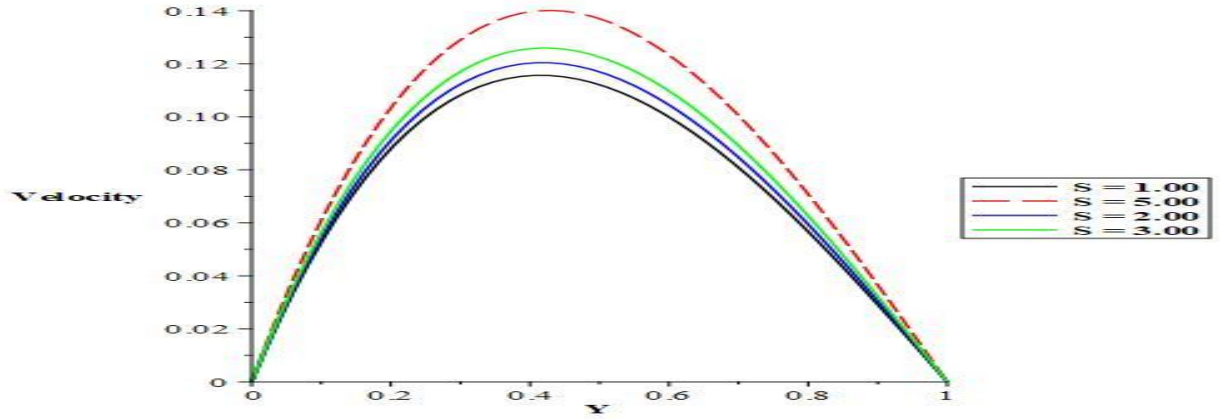

Figure 4: Effect of S on velocity profiles.

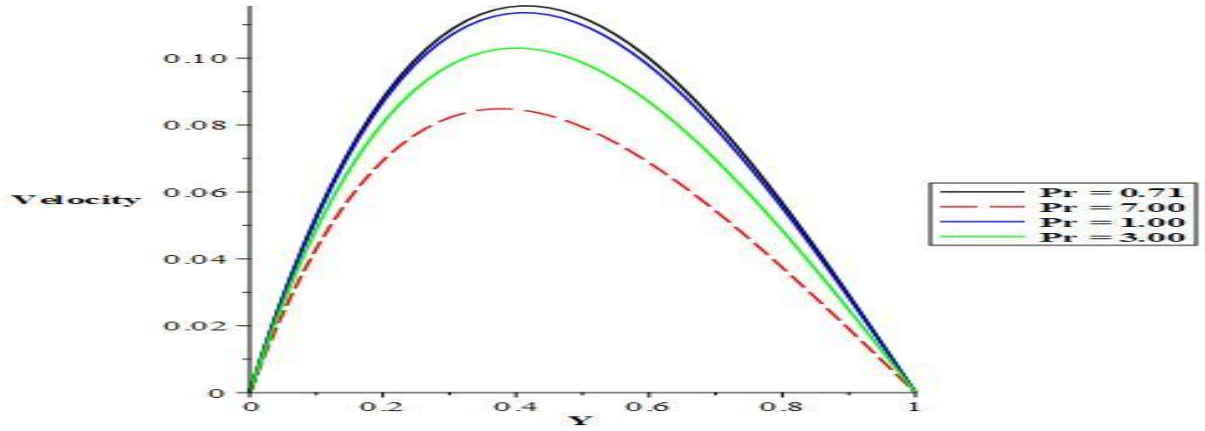

Figure 5: Effect of Pr on velocity profiles.

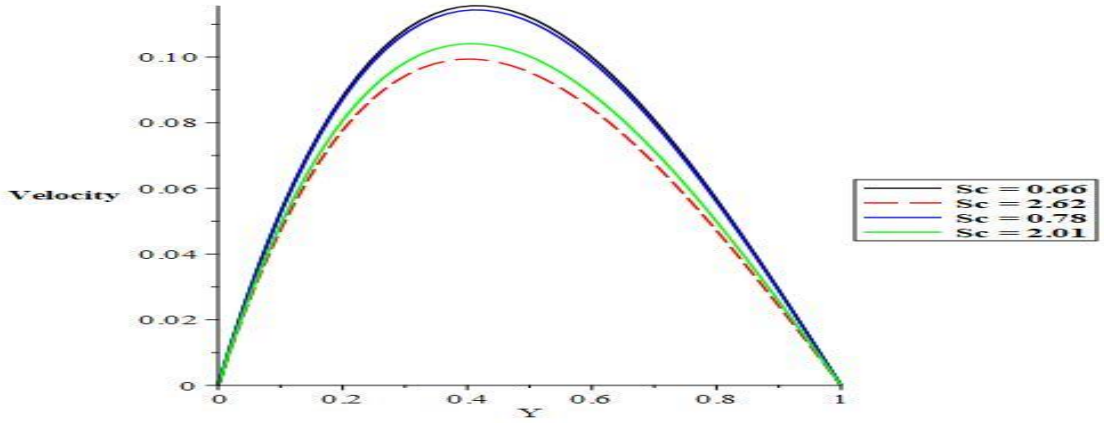

Figure 6: Effect of Sc on velocity profiles.

Figure 7 depict the effect of Prandtl number on the temperature profiles. From this Figure, it is clear that the temperature becomes lower as Prandtl number is increased. The effect of heat source on the velocity profiles in the boundary layer is provided in Figures 8. It is viewed that, increase in the heat source parameter causes rise in the momentum boundary layer of the fluid.

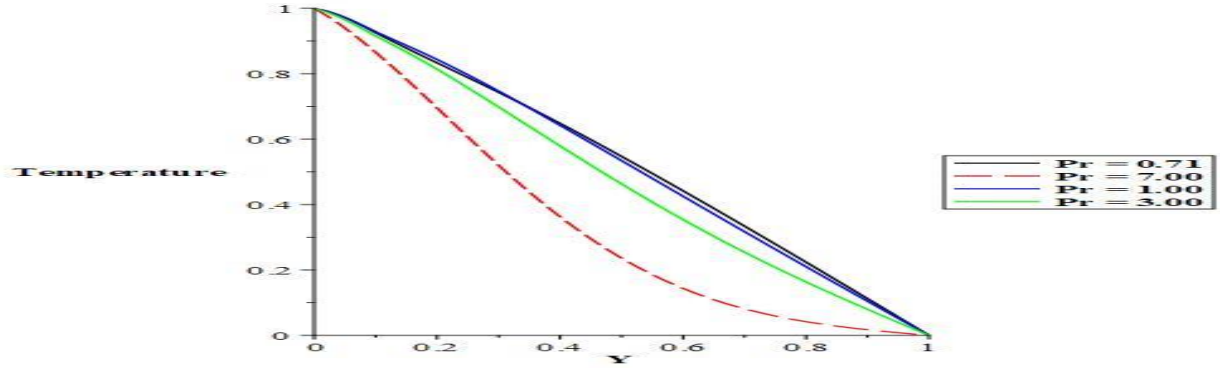

Figure 7. Effect of Pr on Temperature profiles.

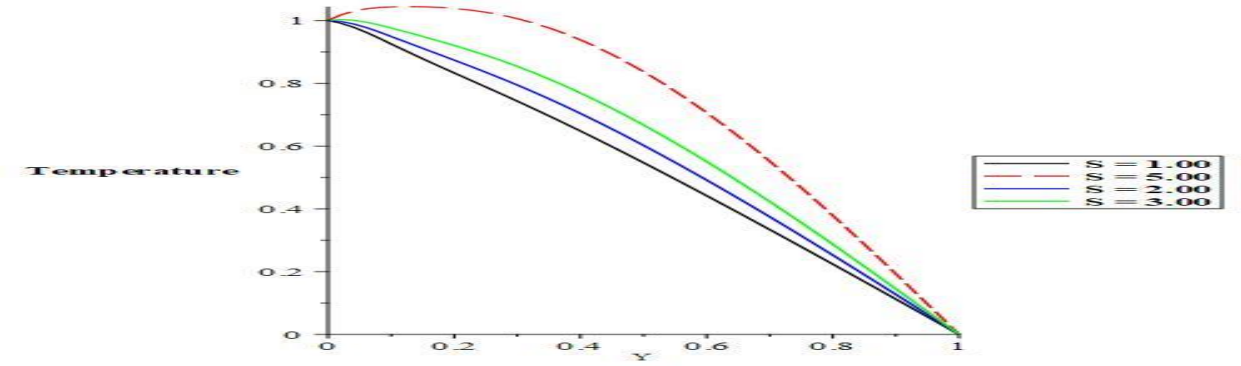

Figure 8: Effect of S on Temperature profiles.

Figures 9 and 10 give the concentration field because of variation in Schmidt number and chemical reaction parameter. It is understood that; the concentration of the fluid falls as the Schmidt number is increased and a similar trend is seen as chemical reaction rises. Physically, this occurs because increase in Sc means decrease of molecular diffusivity, which results in decrease of concentration boundary layer. Hence, the concentration of species is smaller for higher values of Sc.

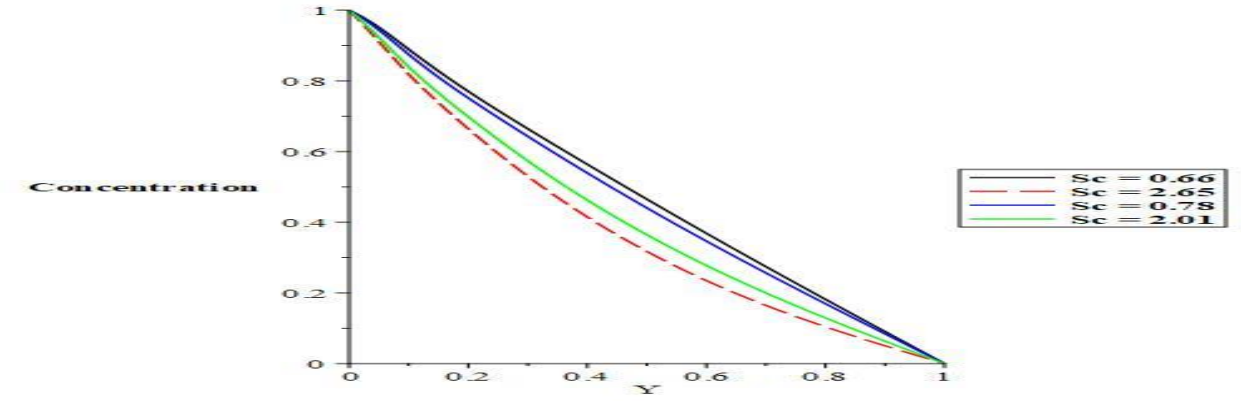

Figure 9: Effect of Sc on concentration profiles.

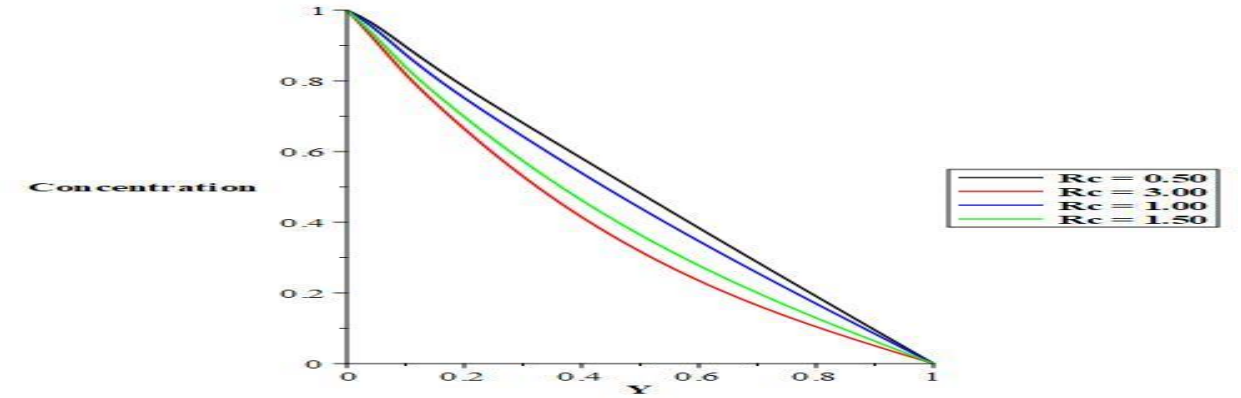

Figure 10: Effect of Rc on concentration profiles.

5.0 CONCLUSION

We have analyzed unsteady MHD convective Couette flow with heat source. The problem is described by a system coupled linear PDEs and solved by FEM. Numerical computations are carried out to understand the effects of physical parameters on the velocity, temperature and

concentration of the fluid. From this study, we deduce the following:

i. The fluid velocity and concentration falls due to higher values of Schmidt number.
ii. The momentum boundary layer is booted significantly for higher values of heat source while a similar trend is also observed a.
iii. Increasing mass and thermal Grashof numbers boost the velocity profile while the fluid temperature reduces as the value of Prandtl number rises.
iv. The velocity and temperature of the fluid reduces for higher values of Pr and M.

ACKNOWLEDGEMENT

The authors appreciate the financial support received from the Tertiary Education Trust Fund (TETFund), Nigeria through Federal University Gusau, Nigeria Institutional Based Research (IBR) with grant allocation number "TETF/DR&S/CE/UNIV/GUSAU/IBR/2020/VOL.I" .

REFERENCES

Anwar, T., Kumam, P., Shah, Z., Watthayu, W., & Thounthong, P. (2020). Unsteady radiative natural convective MHD nanofluid flow past a porous moving vertical plate with heat source/sink. *Molecules*, *25*(4), 854; doi:10.3390/molecules25040854

Ajibade, A. O. and Bichi, Y. A. (2019). Variable fluid properties and thermal radiation effects on natural convection Couette flow through a vertical porous channel. Journal of Advances in Mathematics and Computer Science, 31(1), 1-17.

Bilal, M., Khan, S., Ali, F., Arif, M., Khan, I. and Nisar, K. S. (2021). Couette flow of viscoelastic dusty fluid in a rotating frame along with the heat transfer. Scientific Reports, 11(506), 1 – 16.

Das, S. S. and Bera, N. C. (2014). Hydromagnetic convective Couette flow in presence of time dependent suction and radiative heat source. International Journal of Engineering and Applied Sciences, 1(3), 39 – 44.

Job, V. M., and Gunakala, S. R. (2015). Finite element analysis of unsteady radiative MHD natural convection Couette flow between permeable plates with viscous and joule dissipation. International Journal of Pure00 and Applied Mathematics, 99(2), 123 – 143.

Kesavaiah, D. C., Satyanarayana, P. V., & Sudhakaraiah, A. (2013). Effects of radiation and free convection currents on unsteady Couette flow between two vertical parallel plates with constant heat flux and heat source through porous medium. International Journal of Engineering Research, 2(2), 113-118.

Loganathan, C., & Gomathi, S. Unsteady Three-Dimensional MHD Dusty Couette Flow through Porous Plates with Heat Source. Asian Journal of Applied Sciences, 4(2), 59 – 76.

Raju, R. S., Reddy, G. J., Rao, J. A. and Rashidi, M. M. (2016). Thermal diffusion and diffusion thermo effects on an unsteady heat and mass transfer Magnetohydrodynamic natural convection Couette flow using FEM. Journal of Computational Design and Engineering, 3, 349 – 362.

Rao, K. R., Murthy, M. V. R. and Naik, S. Hari Singh (2014). Thermal radiation effect on an unsteady MHD natural convection Couette flow with heat and mass transfer. International Journal of Computers and Technology, 12(8), 3786 – 3802.

Reddy, G. J., Raju, R. S., Rao, J. A. and Gorla, R. S. R. (2017). Unsteady MHD heat transfer in Couette flow of water at 4oC in a rotating system with ramped temperature via finite element method. International Journal of Applied Mechanics and Engineering, 22(1), 145 – 161.

Seth, G. S., Sharma, R., & Kumbhakar, B. (2016). Effects of Hall current on unsteady MHD convective Couette flow of heat absorbing fluid due to accelerated movement of one of the plates of the channel in a porous medium. Journal of Porous Media, 19(1). DOI:1615/JPorMedia.v19.i120

Sharma, T., Sharma, P., & Kumar, N. (2021). Entropy generation in thermal radiative oscillatory MHD Couette flow in the influence of heat source. International Journal of Physics: Conference Series (Vol. 1849, No. 1, p. 012023). IOP Publishing.

Sharma, T., Sharma, P., & Kumar, N. (2022). Study of dissipative MHD oscillatory unsteady free convective flow in a vertical channel occupied with the porous material in the presence of heat source effect and thermal radiation. International Journal of Physics: Conference Series (Vol. 2178, No. 1, p. 012012). IOP Publishing.

Sukumar, M. and Varma, S. V. K. (2016). Entropy generation and temperature dependent heat source effects on MHD Couette flow with permeable base in the presence of radiation and viscous dissipation. Middle-East Journal of Scientific Research, 24 (8), 2577 – 2588.

Xia, W. F., Animasaun, I. L., Wakif, A., Shah, N. A., & Yook, S. J. (2021). Gear-generalized differential quadrature analysis of oscillatory convective Taylor-Couette flows of second-grade fluids subject to Lorentz and Darcy-Forchheimer quadratic drag forces. International Communications in Heat and Mass Transfer, 126, doi/10.106/j.icheatmasstransfer.2021.105395.